Journal of the Serbian Chemical Society
JSCS@tmf.bg.ac.rs • www.shd.org.rs/JSCS
J. Serb. Chem. Soc. *87* (5) 561–573 (2022)
JSCS–5541
Original scientific paper
Published 18 February 2022

New rhodium(III)–ED3AP complex: Crystal structure, characterization and computational chemistry

MARKO D. RADOVANOVIĆ[1#], MARIJA S. RISTIĆ[1#], MATIJA ZLATAR[2#], FRANK W. HEINEMANN[3] and ZORAN D. MATOVIĆ[1]*

[1]*University of Kragujevac, Faculty of Science, Department of Chemistry, Radoja Domanovića 12, 34000 Kragujevac, Serbia,* [2]*University of Belgrade – Institute of Chemistry, Technology and Metallurgy, Njegoševa 12, 11000 Belgrade, Serbia and* [3]*University Erlangen-Nürnberg (FAU), Department of Chemistry and Pharmacy, Inorganic Chemistry, Friedrich-Alexander, Egerlandstraße 1, 91058 Erlangen, Germany*

(Received 30 December 2021, revised 14 January, accepted 15 January 2022)

Abstract: Only one (*trans*(O_5)-Na[Rh(ED3AP)]·3H_2O) of possible two isomers was synthesized and characterized by single crystal X-ray analysis, IR and UV–Vis spectroscopy. Computational analysis of both isomers was performed with three levels of theory (B3LYP/TZV, BP86/TZV, OPBE/TZV), which gave consistent results. The more stable isomer by total energy and ligand field stabilization energy (LFSE) was *trans*(O_5) which appeared in synthesis. The calculation of excited state energies complied with UV–Vis spectra, especially with OPBE functional. The results of excited state energy pointed out the differences among isomers in means of a splitting pattern of $^1T_{2g}$ excited state term. Both isomers have a strongly delocalized structure, according to the natural bonding orbital (NBO) analysis. NBO analysis shows that the *trans*(O_5) isomer is more stable than *trans*(O_5O_6) for approx. 87 kJ/mol. Therefore, only the *trans*(O_5) isomer is present in the reaction mixture.

Keywords: rhodium; EDTA; crystal structure; NBO; LFDFT.

INTRODUCTION

Metal complexes with EDTA-type of ligands (EDTA = ethylenediamine--*N*,*N*,*N'N'*-tetraacetate) are used in laboratory settings,[1] industrial processes,[2] in medicine,[3–5] environmental field[6,7] and biological systems.[8,9] The rhodium(III) and its complexes with EDTA-type ligands have been extensively investigated for many decades.[10–14] When it comes to the ED3AP ligand (ethylenediamine--*N*,*N*,*N'*-triacetato-*N'*-3-propionato anion), one cannot say that it is thoroughly investigated. The unsymmetrical hexadentate ED3AP ligand can form two geo-

* Corresponding author. E-mail: zmatovic@kg.ac.rs
# Serbian Chemical Society member.
https://doi.org/10.2298/JSC211230003R

metrical isomers depending on the position of the six-membered chelate rings: *trans*(O_5) and *trans*(O_5O_6) (Fig. 1). The literature data show that *trans*(O_5) ED3AP isomer is more stable of the two in the case of Co(III),[15] Cr(III),[16] Cu(II)[17] and Ni(II)[18] complexes. This outcome is explained by the low strain in the equatorial plane at the *trans*(O_5) isomer because the in-plane 5-5-6 the arrangement of the chelate rings makes the propionate ring less strained than the acetate ones. The six-membered propionate ring serves better for the formation of the less-strained ring in equatorial plane favouring the *trans*(O_5) isomer of $[Rh(ED3AP)]^-$ complexes, with 5-5-6 in-plane arrangement of rings.

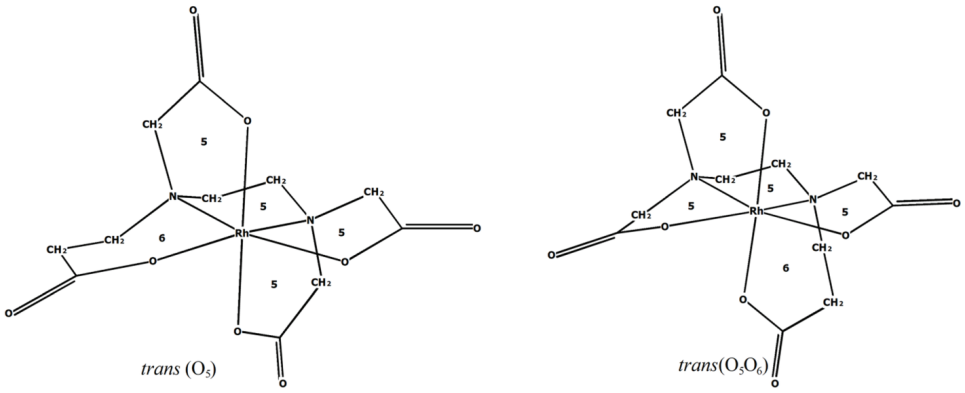

Fig. 1. Two possible geometrical isomers of the $[Rh(ED3AP)]^-$ complex. The size of chelate rings (five- or six- membered) is indicated.

Rhodium complexes are an important alternative to platinum-based complexes in cancer therapy. Many half-sandwich complexes of Rh have been reported with promising results,[19–21] as well as the octahedral rhodium complexes.[22,23] Also, rhodium complexes are known as antimicrobial agents.[24–27] However, there is insufficient data on the antitumor and the antimicrobial activity of rhodium complexes containing EDTA type of ligand.[11] Bearing this in mind, we have continued our research on complexes of Rh-EDTA type. Thus, in this paper, two isomers (*trans*(O_5) and *trans*(O_5O_6)) of $[Rh(ED3AP)]^-$ complex are investigated. In this paper a new rhodium (III) complex has been reported: $Na[Rh(ED3AP)]\cdot 3H_2O$. The IR, and UV–Vis spectra were discussed in relation to the geometry of the complex. Molecular mechanics and density functional theory (DFT) methods have been used to model the most stable geometric isomer and significant structural and energetic data were obtained. natural bonding orbital (NBO)[28] analysis is used to get insight into the energetics of these Werner-type of complexes. Ligand field density functional theory (LFDFT)[29] has been used to calculate the ligand field (LF) parameters and the excited state energies and rationalize the differences between two isomers.

EXPERIMENTAL

Reagents and physical measurements

All chemicals were purchased from Sigma–Aldrich and were used without any further purification. H_4ED3AP was prepared using a previously described procedure.[18] Elemental (C, H, N) analysis of the sample was carried out in the Center for Instrumental Analysis, Faculty of Chemistry, Belgrade. IR spectra (in KBr pellets) were recorded on a Perkin Elmer FT-IR spectrophotometer Spectrum One. Electronic absorption spectra were obtained using a double beam UV–Vis spectrophotometer model Cary 300 (Agilent Technologies, Santa Clara, CA, USA) with 1.0 cm quartz cells. The melting point was measured by the Stuart melting device with accuracy ±1 °C.

Preparation of the complex

The complex has been prepared by the previously reported procedure.[11] After elution with 0.1 mol dm^{-3} NaCl, a main yellow band was detected on the chromatographic column. The yellow band eluate was separated, evaporated, desalted using Sephadex G-10 resin and evaporated to 5 cm^3. After adding of 3 to 4 cm^3 of ethanol, the solution was left in a refrigerator for several days. After several days, the yellow crystals of the band were collected and air-dried. Yield: 0.15 g (6.22 %). Melting point: > 305 °C. Anal. Calc. for $C_{11}H_{20}N_2NaO_{11}Rh$ (482.19 g mol^{-1}): C, 27.40; H, 4.18; N, 5.81 %. Found: C, 27.50; H, 4.10; N, 5.76 %. IR (KBr, ν_{max} / cm^{-1}): 1664 ν(COO^-), 1623 ν(COO^-), 1567 ν(COO^-), 3475 ν(N–H). UV–Vis (H_2O, c = = 10^{-3} mol dm^{-3}): λ_{max} / nm (ε / dm^3 mol^{-1} cm^{-1}): 295(*sh*) (432), 343 (693).

X-ray crystallographic analysis

Details of crystal data, data collection, and refinement for *trans*(O_5)-Na[Rh(ED3AP)]·$3H_2O$ complex are given in Table S-I of the Supplementary material to this paper. The intensity data were collected using MoKα radiation (λ = 0.71073 Å) on a Bruker–Nonius Kappa CCD diffractometer, graphite monochromator. The data were corrected for Lorentz and polarization effects and the semiempirical absorption corrections were performed based on multiple scans using SADABS V2.06.[30] The structure was solved by direct methods (SHELXTL NT 6.12)[31] and refined by full-matrix least-squares procedures on F2 using SHELXL2016/6.[32] All non-hydrogen atoms were refined anisotropically. The positions of all hydrogen atoms were derived from a difference Fourier map, and their positional parameters were refined. The isotropic displacement parameters of all H atoms were tied to those of their corresponding carrier atoms by a factor of 1.2 or 1.5. Olex2 was used to prepare material for publication.[33]

Computational details

Geometries for Rh (III) complexes were optimized using Gaussian 16 C01 program (G16).[34] The Becke three-parameter exchange functional was employed in this study in conjunction with the Lee–Yang–Parr correlation hybrid functional (B3LYP)[35] and the TZVP basis set.[36] The systems were treated in restricted formalism. The calculations were done with polarizable continuum model (PCM), with water as a solvent, as implemented in the G16. The calculated structures were verified as local minima (all positive eigenvalues by frequency analysis). Starting geometries were taken either from the experimental X-ray structures or were pre-optimized using molecular mechanics. NBO employed in the Gaussian 16 C01 program was used with the same method/basis set, and for natural molecular orbital analysis, we used NBO 7.0.[28] We used the LFDFT to calculate excited state energies on either optimized or X-ray geometries. The LFDFT consists of four steps. Firstly, we performed an average of configuration (AOC) calculation, a spin-restricted calculation with 6 electrons distributed evenly

over 5 Kohn–Sham (KS) orbitals with dominantly Rh(III) 4d character. Using those AOC KS orbitals, in the second step, we calculated energies of all 210 Slater determinants (SD) originated from the d^6 configuration in a spin-unrestricted way. These SD energies were then used to determine the parameters of inter-electron repulsion (Racah's parameters) and eigenvalues, of the one-electron effective ligand-field (LF) Hamiltonian. These parameters were in the final step used to determine the excited state energies by diagonalizing the total LF Hamiltonian in the basis of SDs. LFDFT procedure was obtained using Amsterdam density functional (ADF)[37] program with three different functionals (B3LYP[35], BP86[38] and OPBE[39]) and Slater type TZP basis set. AOC calculations were performed with water included as a solvent through the conductor-like screening model (COSMO).

RESULTS AND DISCUSSION

Synthesis and spectral analysis of complexes

The hexadentate ED3AP ligand was used for the synthesis of the new *trans*(O_5)-[Rh(ED3AP)]$^-$ complex. The preparation of the ligand was reported previously.[18] The reaction between the equimolar amounts of $RhCl_3 \cdot 3H_2O$ and ED3AP in the water at 145 °C, was carried out, and column chromatography was used to separate the complex as described above. The corresponding rhodium (III) complex was obtained, as yellow crystals of *trans*(O_5)-Na[Rh(ED3AP)]·$3H_2O$ suitable for X-ray analysis. The complex was also characterized by elemental analysis, IR, UV–Vis, spectroscopy and single-crystal X-ray diffraction studies.

The carboxylate asymmetric stretching frequencies have been used as a criterion for distinguishing protonated (1700–1750 cm^{-1}) and coordinated carboxylate (1560–1680 cm^{-1}). The carboxylate asymmetric stretching of five-membered chelate rings are at higher energy (1600–1680 cm^{-1}) than the corresponding ones of six-membered chelate rings (1560–1600 cm^{-1}). The complex shows two high intensity band at 1664 and 1623 cm^{-1}, and these are assigned to asymmetric vibrations of the five-membered acetate rings in-plane and out-of-plane respectively (Fig. S-1, Supplementary material). The same complex shows one high intensity band at 1567 cm^{-1}, assigned to the carboxylate group of the six-membered in-plane 3-propionate ring. The absence of other vibrations in the 1700–1750 cm^{-1} area suggests that all carboxylate groups are coordinated.

Data of the UV–Vis spectra of the complex are presented in Fig. 2.

We also gave spectra of the *trans*(O_5)-[Rh(eddadp)]$^-$ complex[14] for comparison. The shapes of both spectra show two bands arising from the spin-allowed transitions ($^1A_{1g} \rightarrow {}^1T_{1g}$ and $^1A_{1g} \rightarrow {}^1T_{2g}$ in O_h assignment), but there are minor differences among them. *trans*(O_5)-[Rh(eddadp)]$^-$ has higher in energy transitions (lower wavelength) due to the stronger ligand field surrounding of the equatorial plane of the 656 chelate ring system, contrary to the 556 chelate ring system of our complex.

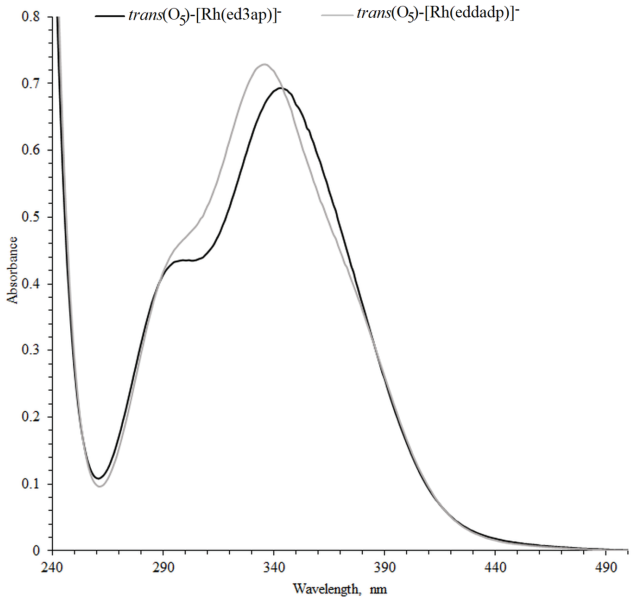

Fig. 2. Electronic absorption spectra of Rh(III) complexes in aqueous solution (c = 10^{-3} mol dm^{-3}): ━, *trans*(O_5)-[Rh(ED3AP)]$^-$ and ═, *trans*(O_5)-[Rh(eddadp)]$^-$.[14]

Description of the crystal structures

The structural diagram of the *trans*(O_5)-Na[Rh(ED3AP)]·3H_2O along with the packing in the crystals is illustrated in Fig. 3. Selected bond distances are listed in Table S-II, Supplementary material. The asymmetric unit contains one formula unit, comprising two moieties: the negatively charged rhodium complex [Rh(ED3AP)]$^-$ and Na^+ coordinated to three water molecules. Therefore, the orthorhombic unit cell contains eight units: four cations and four anions. The four cationic species (Na^+) are partially (triply) hydrated. The

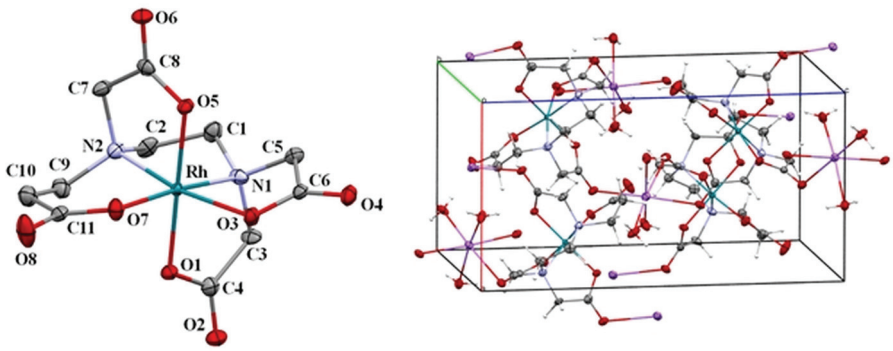

Fig. 3. Ortep diagram of the *trans*(O_5)-[Rh(ED3AP)]$^-$ complex anion and crystal packing view along *b* axis (50% probability ellipsoids).

trans(O_5) geometry of [Rh(ED3AP)]$^-$ entity contains Rh(III) center in a well approximated octahedral geometry. The rhodium(III) ion coordinates six donor atoms from the ligand: four deprotonated carboxylic oxygens and two amine nitrogen atoms.

The equatorial positions of the coordination octahedron are occupied by two deprotonated carboxylic oxygens (Rh-O3 2.053(2) Å, Rh-O7 2.043(2) Å) and the two nitrogen atoms of the ligand (Rh-N1 2.011(2) Å, Rh-N2 2.023(2) Å). The axial positions are occupied by two oxygen donor atoms of the third and fourth carboxyl (Rh-O5 2.006(2) Å, Rh-O1 1.999(2) Å). The second oxygen atom of the acetic in-plane carboxylic group interacts with the sodium ion (O4-Na1 2.516(2) Å). The Rh-ligand bond distances and angles (Table S-II) are comparable with the corresponding ones of analogous complexes.[10–13] The ethylenediamine E ring is in a twisted conformation. The puckering parameters are $q2$ = 0.452(2) Å and $\varphi 2$ = 266.6(2)°. The ideal values for a twisted conformation are $q2$ > 0 Å, $\varphi 2$ = 90°.[40] One of the five-membered rings adopted an envelope conformation, while the other two five-membered acetate rings are in a twisted conformation. Their puckering parameters are $q2$ = 0.122(2) Å, $\varphi 2$ = 183.1(1)° (RhO1C4C3N1), $q2$ = 0.474(2) Å, $\varphi 2$ = 157.4(3)° (RhO3C6C5N1) and $q2$ = 0.151(2) Å, $\varphi 2$ = = 162.1(9)° (RhO5C8C7N2). The equatorial six-membered propionate ring is in a half-chair conformation (RhN2C9C10C11O7) with puckering parameters: $q2$ = 0.362(2) Å, $q3$ = –0.382(2) Å, $\varphi 2$ = 110.1(3)°, θ = 136.5(2)°.

Computational chemistry

LFDFT. We used three different exchange-correlation functionals (BP86, OPBE, B3LYP) for AOC and SD calculations to determine the excited state energies through the LFDFT procedure on X-ray and B3LYP/TZVP optimized geometries. According to the Tanabe-Sugano diagram, the octahedral (O_h) low-spin d^6 complexes, such as Rh(III)-EDTA type complexes, give rise to two low spin excited states: $^1T_{1g}$ lower and $^1T_{2g}$ higher in energy. Both isomers (*trans*(O_5) and *trans*(O_5O_6)) of [Rh(ED3AP)]$^-$ complex are in octahedral coordination but with lower true symmetry (C_1 point group). Complexes have two N and two O donor atoms in the equatorial position, higher in the spectrochemical series than two axial O donor atoms. Because of that, Rh(III)-EDTA type complexes have a splitting pattern corresponding to D_{4h} symmetry (*i.e.*, holohedrized D_{4h} symmetry). Due to the unequal ligand surrounding in equatorial and axial positions, the lower energy $^1T_{1g}$ term is split to double degenerated ^1E_g and non-degenerated $^1A_{2g}$. The higher energy $^1T_{2g}$ term splits to double degenerate ^1E_g and non-degenerated $^1B_{2g}$ (Scheme S-1, Supplementary material).

In the case of ideal D_{4h} symmetry, a splitting pattern of four terms as described above is expected. In actual symmetry (C_1), which is contained in the non-empirical LF Hamiltonian, complete degeneracy removal is expected. This is

what is observed in LFDFT calculations (Table I). Still nearby in energy excitations may be considered as belonging to the degenerate ^1E_g term. The results of LFDFT calculation and their comparison with the experimental values of excited state energies for *trans*(O_5) isomer, which are also reported in this work, are given in Table I. As a consequence of the proximity of split transitions, only two are experimentally observed of the expected four. The average of three calculated values of the particular transition ($^1A_{1g}\rightarrow{}^1T_{1g}$ or $^1A_{1g}\rightarrow{}^1T_{2g}$) is compared with the experimental one, and the comparison is given as absolute error (AE, Table I). Considering the mean absolute error (MAE), we concluded that the results of OPBE functional are excellent on the X-ray geometry. The results are less accurate on B3LYP optimized structure no matter which functional is used. The geometry optimization by B3LYP overestimates metal-ligand bond distances (Table S-III, Supplementary material) and therefore LFDFT gives slightly lower energies of the excited states. These results indicate the importance of geometry used for excited state calculations. It is noteworthy that LFDFT calculations on B3LYP geometries are still accurate within 2000 cm^{-1}.

TABLE I. Energies (10^3 cm^{-1}) of the singlet electronic states from LFDFT and comparison with available experimental data

[Rh(ED3AP)]$^-$	Electronic state									
	trans(O_5)[a]				*trans*(O_5)[b]			*trans*(O_5O_6)[b]		
	B3LYP	BP86	OPBE	Exp.	B3LYP	BP86	OPBE	B3LYP	BP86	OPBE
$^1A_{1g}\rightarrow{}^1T_{1g}$	28.18	27.77	27.60	29.15	26.01	25.69	25.48	25.55	25.29	25.10
	28.63	28.27	28.15		26.42	26.13	25.97	25.82	25.54	25.36
	30.89	30.18	29.87		28.52	27.79	27.47	27.58	27.10	26.72
$^1A_{1g}\rightarrow{}^1T_{2g}$	35.54	34.19	33.59	33.90	33.35	32.22	31.61	31.85	31.57	30.94
	36.41	34.94	34.33		34.27	33.01	32.39	33.56	33.36	32.58
	37.84	36.60	35.98		35.37	34.33	33.73	34.47	34.56	33.82
AE ($^1A_{1g}\rightarrow{}^1T_{1g}$)	0.08	0.42	0.62		2.17	2.62	2.85			
AE ($^1A_{1g}\rightarrow{}^1T_{2g}$)	2.69	1.34	0.73		0.43	0.71	1.33			
MAE	1.39	0.88	0.67		1.30	1.67	2.09			

[a]X-ray structure; [b]B3LYP/TZVP optimized structure

We presented results from Table I in the form of a chart (Fig. 4) only for the optimized structures to discuss the relationship between the geometric isomers and the energies of their excited states and their splitting pattern.

There is no significant difference in the splitting of the excited states originating from $^1T_{1g}$ (lower in energy) in the case of both isomers. But the splitting of the $^1T_{2g}$ (higher in energy) term seems to be more related to the type of isomer. The ^1E_g ($^1T_{2g}$) is lower in energy than $^1B_{2g}$ in the case of the *trans*(O_5) isomer. In the case of the *trans*(O_5O_6), the opposite is observed. Furthermore, in *trans*(O_5O_6), the ^1E_g ($^1T_{2g}$) state is split more.

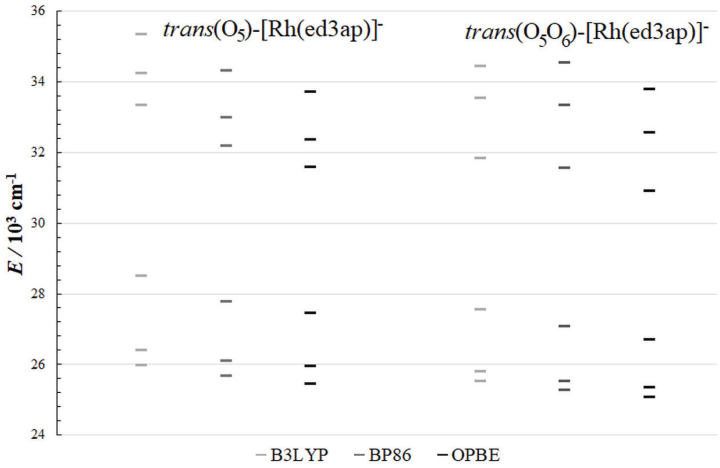

Fig. 4. Excited state energies of B3LYP/TZVP optimized structures for *trans*(O_5) and *trans*(O_5O_6) isomers of [Rh(ED3AP)]$^-$ complex obtained by LFDFT.

The calculation of the single-point (SP) energies by different exchange-correlation functionals (B3LYP, BP86, OPBE) were performed in order to interpret the stability of discussed isomers. SP energies were obtained on B3LYP optimized structures as well as $\Sigma\Delta(O_h)$ value. This parameter represents geometry distortion of the complex from the ideal octahedron. We also calculated the ligand field stabilization energy (LFSE) and collected all results in Table II. *trans*(O_5) isomer, with a 556-55 system of chelate rings, which is more adjustable to octahedral geometry and has lower value of $\Sigma\Delta(O_h)$ than *trans*(O_5O_6) isomer with his 555-56 system of chelate rings. The *trans*(O_5O_6) isomer has a higher value of LFSE (less stabilization) than the *trans*(O_5) isomer because of the more significant angle distortion. Consequently, the t_{2g} set (d_{xy}, d_{xz}, d_{yz}) is higher in energy. The more stable isomer is *trans*(O_5) because of LFSE's contribution to the total energy. The less stable *trans*(O_5O_6) isomer has not been isolated in the synthesis. All the results presented in Table II, are independent of the choice of exchange-correlation functional.

TABLE II. Relative and ligand field stabilization energies (E / kJ mol^{-1}) of optimized [Rh(ED3AP)]$^-$ isomers

Isomer	Ring system	$\Sigma\Delta(O_h)$[a]	State					
			B3YLP		BP86		OPBE	
			ΔE[b]	LFSE[c]	ΔE[b]	LFSE[c]	ΔE[b]	LFSE[c]
trans(O5)-[Rh(ED3AP)]$^-$	556–55	44	0.00	–406.26	0.00	–400.07	0.00	–398.55
trans(O5O6)-[Rh(ED3AP)]$^-$	555–56	66	24.49	–398.55	20.79	–392.52	24.70	–391.11

[a]The sum of the absolute values of the deviations from 90° of the twelve L–M–L' angles; [b]the isomer with the lowest energy minimum has been indicated with 0 kJ mol^{-1}; [c]ligand field stabilization energy in kJ mol^{-1}

NBO. NBO outputs from the Gaussian calculations were analyzed using the NBO 7.4 package. The empirical regularities in ML_n stoichiometry for d-block elements suggest a Rule of 12 ("duodectet rule"), governed by six d-block valence orbitals (one s plus five d), analogous to the four p-block counterparts (one s plus three p). Therefore, the idealized sd^{μ} hybrids for transition metal bonding (equivalent to sp^{λ} hybrids for main-group bonding) is proposed. NBO analysis exhibits duodectet-conforming Lewis-like bonding patterns for transition metal species throughout the d-block. According to the NBO procedure, the formation of a diatomic molecule leads to the key orbital transformation: NAO (natural atomic orbital) → NHO (natural hybrid orbital) → NBO. These NHOs present the key point in building NBOs and NLMOs (natural localized molecular orbitals) and will be evaluated in this paper. Within both molecules, there are three σRh-L 2c NBO pairs. These pairs enable bonding of Rh(III) with two nitrogens and one carboxylate oxygen. The rhodium bonds are highly polarized and according to the hybrid coefficients (*h*) of the Rh(III) ion, sd^2 hybridization may be deduced. This hybridization requires an M–L angle of 90°, which is satisfied in our case. It may be seen that BD Rh1-O5 orbital is stabilized by more than 80 kJ/mol, with respect to the other two BD Rh-N orbitals. These Rh(III)–L bonds are highly polarized with limited total orbital participation of Rh(III) (around 20 %). The polarity of the BD NBOs is best described by the "natural ionicity para-

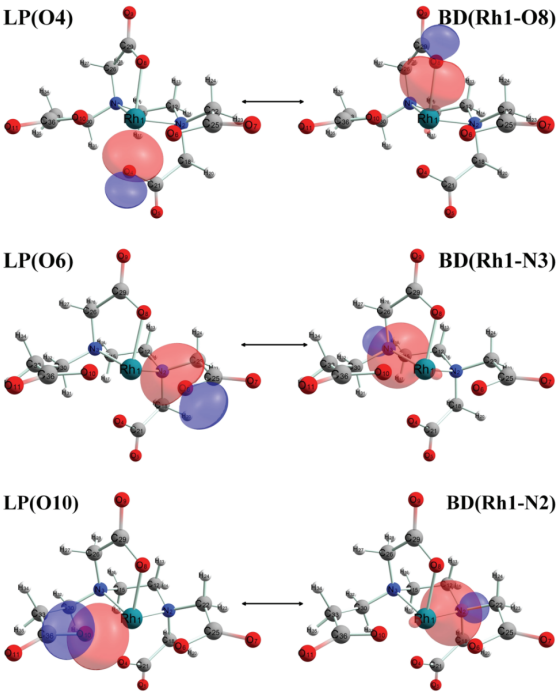

Fig. 5. 3-Center, 4-4lectron L:–Rh–:L' hyperbond orbitals.

meter, i_{AB}. One may ask about the other ligating atoms from ED3AP chelate. The answer that NBO offers might be dual. First, the NBO analysis does find three strong 3-center 4-electrons rhodium-ligand hypervalent bonds ("ω-bonding", Fig. 5 and Table III). As shown in Table III, each such 3c/4e L:–Rh–:L' ω-bond can be formulated in terms of distinct L + RhL' and LRh + L' resonance structures, each conforming to the 12e duodectet rule, but appearing in composite resonance-hybrid form as a 14e "hypervalent" species. However, the complex unit in whole corresponds to the 18e hypervalent center involving three 3c/4e ω bonds.

TABLE III. 3-Center, 4-Electron L:–Rh–:L' hyperbonds (L–Rh:L' <=> L:Rh–L')[a] of $[Rh(ED3AP)]^-$ isomers; threshold for detection: 33.3 %

Orb.	Hyperbond L : –Rh– : L'	L–Rh+:L', % / :L+Rh–L', %	OCC, electrons
		trans(O_5)	
1.	N 2 :–Rh 1– : O 10	56.1 / 43.9	3.9328
2.	N 3 : –Rh 1– : O 6	56.6 / 43.4	3.9390
3.	O 8 : –Rh 1– : O 4	50.3 / 49.7	3.9386
		trans(O_5O_6)	
1.	N 2 : –Rh 1– : O 10	58.4 / 41.6	3.9297
2.	N 3 : –Rh 1– : O 6	56.6 / 43.4	3.9258
3.	O 8 : –Rh 1– : O 4	52.6 / 47.4	3.9315

The donor–acceptor diagram depicts a universal quantum mechanical paradigm for energetically stabilizing the superposition of occupied and unoccupied localized orbitals in chemical interactions. As might be expected, the interaction of unperturbed donor $\varphi_i^{(0)}$ (valence LP) with acceptor $\varphi_{j*}^{(0)}$ (valence BD*) leads to the corresponding second-order i→j∗ of stabilization:

$$\Delta E^{(2)}_{i\rightarrow j*} = -2\langle\varphi_i^{(0)}|F|\varphi_{j*}^{(0)}\rangle^2/(\varepsilon_{j*}^{(0)} - \varepsilon_i^{(0)}) \quad (1)$$

For the *trans*(O_5O_6) isomer, this stabilization estimate, $\Delta E^{(2)}_{i\rightarrow i*}$, is 87 kJ/mol lower than for the *trans*(O_5) isomer. This result is in accordance with the calculated SP energies and is one of the reasons for the absence of the *trans*(O_5O_6) isomer in the reaction mixture.

CONCLUSION

We reported the investigation of two isomers (*trans*(O_5) and *trans*(O_5O_6)) of $[Rh(ED3AP)]^-$ complex. Only one of the possible two was synthesized and characterized. We determined the *trans*(O_5)-Na[Rh(ED3AP)]·3H_2O X-ray structure and characterized it by IR, and UV–Vis spectroscopy data of complex as well. We investigated the stability of two isomers by total energy and LFSE using different DFT levels of theory (B3LYP/TZV, BP86/TZV, OPBE/TZV). All DFT calculations are in agreement with each other. The total energy difference between *trans*(O_5) and *trans*(O_5O_6) isomer is beyond boundary energy we rep-

orted in our previous work[10]; therefore, the absence of *trans*(O_5O_6) isomer in the synthesis was expected. We used the same levels of theories for the LFDFT calculation of excited states. All three (B3LYP/TZV, BP86/TZV, OPBE/TZV) gave results in good agreement with the experimental ones (UV–Vis spectra). The best result was obtained with OPBE functional on the X-ray geometry (mean absolute error of only 670 cm^{-1}). By examining the splitting pattern of excited state energies, we determined an obvious difference in splitting the $^1T_{2g}$ term among isomers. In the case of the *trans*(O_5) isomer, the $^1E_g(^1T_{2g})$ term is lower in energy than the $^1B_{2g}$ term. For the *trans*(O_5O_6) isomer opposite is found. The NBO analysis suggests a strongly delocalized structure for both isomers. According to the NBO analysis, the *trans*(O_5) isomer is a more stable one for approx. 87 kJ/mol and the only present in the reaction mixture.

SUPPLEMENTARY MATERIAL

Additional data and information are available electronically at the pages of journal website: https://www.shd-pub.org.rs/index.php/JSCS/article/view/11533, or from the corresponding author on request.

Acknowledgement. This work is supported by the Ministry of Education, Science and Technological Development of Republic of Serbia (Agreement No. 451-03-9/2021-14/200122 and 451-03-9/2021-14/200026).

ИЗВОД

НОВИ РОДИЈУМ(III)–ED3AP КОМПЛЕКС: КРИСТАЛНА СТРУКТУРА, КАРАКТЕРИЗАЦИЈА И КОМПЈУТАЦИОНА ХЕМИЈА

МАРКО Д. РАДОВАНОВИЋ[1], МАРИЈА С. РИСТИЋ[1], МАТИЈА ЗЛАТАР[2], FRANK W. HEINEMANN[3] и ЗОРАН МАТОВИЋ[1]

[1]Универзитет у Крагујевцу, Природно–математички факултет, Институт за хемију, 34000 Крагујевац, [2]Универзитет у Београду, Институт за хемију, технологију и металургију, Његошева 12, 11000 Београд и [2]University Erlangen-Nürnberg (FAU), Department of Chemistry and Pharmacy, Inorganic Chemistry, Friedrich-Alexander, Egerlandstraße 1, 91058 Erlangen, Germany

Један (*trans*(O_5)-Na[Rh(ED3AP)]·3H_2O) од могућа два изомера синтетисан је и окарактерисан применом дифракције X-зрака на монокристалу, IR и UV–Vis спектроскопијом. Компјутерска анализа оба изомера обављена је помоћу три теоријска модела која су дала конзистентне резултате. Стабилнији изомер по укупној енергији и енергији стабилизације лигандног поља (LFSE) је *trans*(O_5) који је и изолован у синтези. Прорачун енергија ексцитованих стања дао је добру усаглашеност са UV–Vis спектром, посебно у случају прорачуна са OPBE функционалом. На основу резултата енергија ексцитованих стања уочене су разлике између изомера у начину цепања $^1T_{2g}$ терма. Оба изомера дају снажно делокализовану структуру судећи по NBO анализи. На основу NBO анализе, *trans*(O_5) изомер је стабилнији за 87 kJ/mol и једини је присутан у реакционој смеши.

(Примљено 30. децембра 2021, ревидирано 14. јануара, прихваћено 15. јануара 2022)

REFERENCES

1. C. Drouza, M. Vlasiou, A. D. Keramidas, *Dalt. Trans.* **42** (2013) 11831 (https://doi.org/10.1039/C3DT50619C)
2. E. Repo, J. K. Warchoł, A. Bhatnagar, M. Sillanpää, *J. Colloid Interface Sci.* **358** (2011) 261 (https://doi.org/10.1016/j.jcis.2011.02.059)
3. M. E. Markowitz, J. F. Rosen, *J. Pediatr.* **119** (1991) 305 (https://doi.org/10.1289/ehp.99107437)
4. K. Sakthithasan, P. Lévy, J. Poupon, R. Garnier, *Clin. Toxicol.* **56** (2018) 1143 (https://doi.org/10.1080/15563650.2018.1478424)
5. G. A. Lamas, O. M. Issa, *Curr. Cardiol. Rep.* **18** (2016) 20 (https://doi.org/10.1007/s11886-015-0690-9)
6. F. G. Kari, W. Giger, *Environ. Sci. Technol.* **29** (1995) 2814 (https://doi.org/10.1021/es00011a018)
7. H. Xue, L. Sigg, F. Günter Kari, *Environ. Sci. Technol.* **29** (1995) 59 (https://doi.org/10.1021/es00001a007)
8. J. Porath, J. Carlsson, I. Olsson, G. Belfrage, *Nature* **258** (1975) 598 (https://doi.org/10.1038/258598a0)
9. J. Carrasco-Castilla, A. J. Hernández-Álvarez, C. Jiménez-Martínez, C. Jacinto-Hernández, M. Alaiz, J. Girón-Calle, J. Vioque, G. Dávila-Ortiz, *Food Chem.* **135** (2012) 1789 (https://doi.org/10.1016/j.foodchem.2012.06.016)
10. M. S. Jeremić, M. D. Radovanović, F. W. Heinemann, M. M. Vasojević, Z. D. Matović, *Polyhedron* **169** (2019) 89 (https://doi.org/10.1016/j.poly.2019.04.053)
11. M. S. Jeremić, H. Wadepohl, V. V. Kojić, D. S. Jakimov, R. Jelić, S. Popović, Z. D. Matović, P. Comba, *RSC Adv.* **7** (2017) 5282 (https://doi.org/10.1039/C6RA26199J)
12. M. S. Jeremić, M. D. Radovanović, F. Bisceglie, V. V. Kojić, R. Jelić, Z. D. Matović, *Polyhedron* **156** (2018) 19 (https://doi.org/10.1016/j.poly.2018.08.075)
13. K. D. Gailey, D. J. Radanović, M. Djuran, B. E. Douglas, *J. Coord. Chem.* **8** (1978) 161 (https://doi.org/10.1080/00958977808073090)
14. D. J. Radanovic, K. D. Gailey, M. I. Djuran, B. E. Douglas, *J. Coord. Chem.* **10** (1980) 115 (https://doi.org/10.1080/00958978008079858)
15. D. J. Radanovic, V. D. Miletic, T. Ama, H. Kawaguchi, *Bull. Chem. Soc. Jpn.* **71** (1998) 1605 (https://doi.org/10.1246/bcsj.71.1605)
16. D. J. Radanović, N. Sakagami, V. M. Ristanović, S. Kaizaki, *Inorganica Chim. Acta* **292** (1999) 16 (https://doi.org/10.1016/S0020-1693(99)00164-4)
17. D. J. Radanovic, T. Ama, D. M. Gurešic, D. M. Ristanovic, D. D. Radanovic, H. Kawaguchi, *Bull. Chem. Soc. Jpn.* **73** (2000) 2283 (https://doi.org/10.1246/bcsj.73.2283)
18. V. D. Miletić, A. Meetsma, P. J. van Koningsbruggen, Z. D. Matović, *Inorg. Chem. Commun.* **12** (2009) 720 (https://doi.org/10.1016/j.inoche.2009.05.029)
19. R. Pettinari, F. Marchetti, C. Pettinari, F. Condello, A. Petrini, R. Scopelliti, T. Riedel, P. J. Dyson, *Dalt. Trans.* **44** (2015) 20523 (https://doi.org/10.1039/C5DT03037D)
20. F. Hackenberg, L. Oehninger, H. Alborzinia, S. Can, I. Kitanovic, Y. Geldmacher, M. Kokoschka, S. Wölfl, I. Ott, W. S. Sheldrick, *J. Inorg. Biochem.* **105** (2011) 991 (https://doi.org/10.1016/j.jinorgbio.2011.04.006)
21. S. Mukhopadhyay, R. K. Gupta, R. P. Paitandi, N. K. Rana, G. Sharma, B. Koch, L. K. Rana, M. S. Hundal, D. S. Pandey, *Organometallics* **34** (2015) 4491 (https://doi.org/10.1021/acs.organomet.5b00475)
22. S. Mollin, R. Riedel, K. Harms, E. Meggers, *J. Inorg. Biochem.* **148** (2015) 11 (https://doi.org/10.1016/j.jinorgbio.2015.01.005)

23. T.-S. Kang, W. Wang, H.-J. Zhong, J.-X. Liang, C.-N. Ko, J.-J. Lu, X.-P. Chen, D.-L. Ma, C.-H. Leung, *Biochim. Biophys. Acta - Gen. Subj.* **1861** (2017) 256 (https://doi.org/10.1016/j.bbagen.2016.11.032)
24. A. Lapasam, V. Banothu, U. Addepally, M. R. Kollipara, *J. Mol. Struct.* **1191** (2019) 314 (https://doi.org/10.1016/j.molstruc.2019.04.116)
25. A. Lapasam, L. Dkhar, N. Joshi, K. M. Poluri, M. R. Kollipara, *Inorg. Chim. Acta* **484** (2019) 255 (https://doi.org/10.1016/j.ica.2018.09.067)
26. L. Shadap, S. Diamai, V. Banothu, D. P. S. Negi, U. Adepally, W. Kaminsky, M. R. Kollipara, *J. Organomet. Chem.* **884** (2019) 44 (https://doi.org/10.1016/j.jorganchem.2019.01.019)
27. S. S. Hassan, *Appl. Organomet. Chem.* **32** (2018) e4170 (https://doi.org/10.1002/aoc.4170)
28. E. D. Glendening, C. R. Landis, F. Weinhold, *J. Comput. Chem.* **34** (2013) 2134 (https://doi.org/10.1002/jcc.23366)
29. M. Atanasov, C. A. Daul, C. Rauzy, *Chem. Phys. Lett.* **367** (2003) 737 (https://doi.org/10.1016/S0009-2614(02)01762-1)
30. *SADABS* v. 2.06, Bruker AXS, Inc., Madison, WI, 2002
31. G. M. Sheldrick, *Acta Cryst. A* **64** (2008) 112 (https://doi.org/10.1107/S0108767307043930)
32. G.M. Sheldrick, *Acta Cryst. C* **71** (2015) 3 (https://doi.org/10.1107/S2053229614024218)
33. O. V. Dolomanov, L. J. Bourhis, R. J. Gildea, J. A. K. Howard, H. Puschmann, *J. Appl. Crystallogr.* **42** (2009) 339 (https://doi.org/10.1107/S0021889808042726)
34. *Gaussian 16, Revision C.01*, Gaussian, Inc., Wallingford CT, 2016 (https://gaussian.com/relnotes)
35. P. J. Stephens, F. J. Devlin, C. F. Chabalowski, M. J. Frisch, *J. Phys. Chem.* **98** (1994) 11623 (https://doi.org/10.1021/j100096a001)
36. M. F. Peintinger, D. V. Oliveira, T. Bredow, *J. Comput. Chem.* **34** (2013) 451 (https://doi.org/10.1002/jcc.23153)
37. G. te Velde, F. M. Bickelhaupt, E. J. Baerends, C. Fonseca Guerra, S. J. A. van Gisbergen, J. G. Snijders, T. Ziegler, *J. Comput. Chem.* **22** (2001) 931 (https://doi.org/10.1002/jcc.1056)
38. J. P. Perdew, *Phys. Rev. B* **34** (1986) 7406 (https://doi.org/10.1103/PhysRevB.34.7406)
39. J. P. Perdew, K. Burke, M. Ernzerhof, *Phys. Rev. Lett.* **77** (1996) 3865 (https://doi.org/10.1103/PhysRevLett.77.3865)
40. D. Cremer, J. A. Pople, *J. Am. Chem. Soc.* **97** (1975) 1354 (https://doi.org/10.1021/ja00839a011).